

Detection of Biomolecules in an Optofluidic Device

Candidate No. 8257V

Supervisor: Prof. Tuomas Knowles

May 2016

Abstract

Optofluidic devices are those which combine the fields of microfluidics and optics. A proof-of-concept liquid-core, liquid-cladding optofluidic waveguide was designed, fabricated, and tested. Such a device would be useful in the detection of biomolecules as light could be confined to the medium containing such molecules. These waveguides would be dynamically tunable, compared to alternatives such as Teflon AF treatment.

A 488 nm laser coupled to an optical fibre, core diameter 400 μm , with numerical aperture 0.39, was used as the light source. Devices tested had channel heights of 50 μm . Water ($n = 1.335$) containing Fluorescein (2mg/ml) was used as the core liquid. Fluorinert FC-40 ($n = 1.291$) was used as the cladding liquid. Methanol ($n = 1.331$) was also used as a cladding liquid. A novel technique for creating a socket for an optical fibre on a microfluidic device was developed.

Light was successfully coupled into the channel. The amount of coupling via total internal reflection was not established. The intensity variation along the channels were measured and it was noted that most light was coupled by direct illumination rather than by TIR. A coupling efficiency was not established.

In order to construct such a device, two phase flow between immiscible FC-40 and Water was achieved. Hydrophilic conditions inside the microfluidic channels, or flow rates greater than $500 \mu\text{l h}^{-1}$ were noted as being the conditions required to overcome the fluid instabilities to achieve this. Devices of height 100 μm were tested, but laminar flow was not established in either case.

Several drawbacks are noted. The optical fibre matched the dimensions of the width of the channel (500 μm) but was four times the height of the channels. The channel geometries were not exploited in order to directly confirm transmission as a waveguide.

Acknowledgements

For their boundless resourcefulness, and willingness to help, I would like to thank my day-to-day supervisor Dr. Pavan Kumar Challa, Dr. Jérôme Charmet, and Ms. Kadi Liis Saar. I have learnt a great deal from their expertise and their feedback throughout the project helped me advance towards my goals. I would also like to thank those in the Knowles group who provided assistance when my luck with equipment seemed to run out.

I would also like to thank Prof. Tuomas Knowles for providing his invaluable insight on some of the challenges of the project as well as for providing the opportunity to undertake this interesting project.

Contents

1	Introduction	5
1.1	Motivation	5
1.2	Aim	6
1.3	Previous Work	6
1.4	Report Structure	6
2	Theory	7
2.1	Fluid Mechanics	7
2.1.1	Pressure Driven Flow	7
2.1.2	Characterising Flow	7
2.1.3	Laminar Flow Patterning	8
2.1.4	Fluid Instabilities	8
2.2	Optical Theory	9
2.2.1	Total Internal Reflection	9
2.2.2	Fluorescence	9
3	Method	11
3.1	Design	11
3.2	Fabrication	13
3.2.1	Lithography	13
3.2.2	PDMS	13
3.2.3	Placement of Optical Fibre	14
3.2.4	Cleaning	16
3.2.5	Plasma Treatment	16
3.3	Infusion	17
3.3.1	Setup	17
3.3.2	Fluids Used	17
3.3.3	Procedure	18
3.4	Optical Setup	19
3.4.1	Lab Microscope	19

3.4.2	Laser Fluorescence Setup	19
3.4.3	Laser Measurements	20
3.4.4	Software	20
4	Results	21
4.1	Fluid Measurements	21
4.1.1	Two Phase Flow	21
4.1.2	Cleanliness	21
4.1.3	Methanol Flow	23
4.2	Optical Measurements	24
4.2.1	Device A	24
4.2.2	Device B	27
4.2.3	Methanol	29
5	Discussion	31
5.1	Two Phase Flow	31
5.2	Optical Measurements	32
5.3	Further Work	33
6	Conclusion	34
Appendices		35
A	Adapting Surface Energies	36
Bibliography		38

Chapter 1

Introduction

Microfluidic devices have become increasingly popular due to how quickly they can be designed and manufactured at low cost compared to previously used materials (silicon)[1]. These devices have many applications in biological and medical research[2]. The field of Optofluidics was created by the integration of microfluidics and optical devices, and this field is one of many benefiting from the continued interplay between science and technology. There are three main types of optofluidic device: those with fluids-in-solids, fluids-in-fluids, and solids (e.g. colloids) in fluids[3].

1.1 Motivation

A liquid-core, liquid-cladding (L^2) optofluidic waveguide could be, in principle, another component in the toolbox of the microfluidics researcher, since it enables the construction of more complex microfluidic devices. Below is a list of some of the reasons why one might want to construct such a waveguide.

- Many biomolecules are contained within a solvent, some of which may diffuse into the cladding liquid if a miscible liquid is used.
- The very nature of a waveguide means that light can be confined to the core fluid in a microfluidic channel, rather than focusing light in region viewed by an objective lens as per traditional fluorescence microscopy.
- A compact, microfluidic fluorescence microscopy setup using an optical fibre as a receiver for the fluorescent light could be constructed[4].
- The dynamical routing of light is possible, for example, by adjusting the flow rates within the device. This allows for the possibility of creating an optical switch, where light could be passed into a series of different detectors at one end of the device.
- Light can be input into a device from a multiwavelength source. This could be used to track the diffusion of a mixture of two different fluorescent species with unique fluorescence spectra.

1.2 Aim

The aim of this project was to build an L^2 optofluidic waveguide. This can be thought of as a liquid optical fibre. TIR was intended to be used as the primary coupling method.

The primary liquids under investigation were Fluorinert FC-40 (a perfluorinated oil) and Water. Methanol was also investigated as a secondary cladding liquid.

When the core and the cladding are immiscible, the refractive index contrast remains constant down the waveguide. However, it is not immediately straightforward to do this, as will be discussed in later chapters. This report outlines the process by which these devices were designed and built as well as displaying the results from testing.

1.3 Previous Work

Optofluidic devices have been investigated since the early 2000s. In 2004, Wolfe et al. constructed a L^2 waveguide[5]. They used aqueous CaCl_2 miscible liquids in order to obtain the refractive index contrast required. In their devices, the refractive index contrast would decrease as the fluids flowed down the channels due to diffusion. Although this is not necessarily undesirable, this project investigated the use of two immiscible liquids, thus maintaining a refractive index contrast throughout the channel. This is desirable as propagation of light can be maintained over longer distances without attempting to control diffusion times.

1.4 Report Structure

Chapter 2 will outline the microfluidics background and theoretical basis behind the experiments conducted. Chapter 3 outlines the methods used. Chapter 4 outlines the results obtained. Chapter 5 will discuss the results presented. Chapter 6 will contain the conclusion.

Chapter 2

Theory

2.1 Fluid Mechanics

2.1.1 Pressure Driven Flow

The devices used throughout the project were driven by pressure. This is known as hydrodynamic flow. A pressure difference ΔP is related to the flow rate Q by:

$$\Delta P = RQ \quad (2.1)$$

where R is the channel resistance.

The resistance is dependent on the geometry of the channel. Rectangular channels were used within the devices on the project. The resistance for these types of channels is given by[2]:

$$R = \frac{12\mu L}{wh^3} \quad (2.2)$$

where μ is the dynamic viscosity of the fluid, L is the length of the channel, h is the height of the channel, and w is the width of the channel.

2.1.2 Characterising Flow

Fluids are complex. Many competing factors influence their behaviour, and it is useful to characterise them using dimensionless numbers which compare the relative strengths of these factors. These are summarised in Table 2.1.

Number	Symbol	Description	Expression
Reynolds	Re	Ratio of inertial forces to viscous forces	$\frac{\rho v L}{\mu}$
Péclet	Pe	Ratio of advective transport rate to diffusive transport rate	$\frac{L u}{D}$

Table 2.1: Dimensionless numbers utilised in order to describe fluid flow[8]. Re & Pe are useful numbers for quantifying flow regimes inside microfluidic devices. ρ is the density, μ is the dynamic viscosity, v is the (characteristic) flow velocity, and L is a typical length of travel of the fluid.

2.1.3 Laminar Flow Patterning

A low Re, high Pe (low diffusion) regime can be exploited to produce Laminar flow patterning (LFP)[6].

For LFP, the width w_i of a fluid in the channel is given by:

$$\frac{w_i}{d} = \frac{Q_i}{Q_T} \quad (2.3)$$

where d is the total width of the channel. Q_i is the flow rate of the liquid whose width is being investigated. Q_T is the sum of the flow rates of the inlet streams. This process is displayed in Fig.2.1.

2.1.4 Fluid Instabilities

To create a waveguide within a device, LFP must be established. However, the fluids within a channel exist in an energy landscape. Instabilities arise which can minimise the energies of the fluids.

The most considerable of these instabilities posed for the devices is the Rayleigh-Plateau instability[7]. This instability is most commonly seen in the formation of droplets from a column of water exiting a tap.

FC40 and Water are immiscible. At the interfaces between these two liquids, small oscillations are present. In the case of the tap, a sufficiently large oscillation will be able to cleave the stream, minimising the surface energy through the formation of spherical droplets. This minimises the surface area, and thus the surface energy.

By considering the surface energies of column (of radius R) and a sphere of fluid of equal volume, it can be shown that it is energetically favourable for spherical droplets to form if they have the radii R' [9]:

$$R' \geq \frac{3}{2\pi} R \quad (2.4)$$

This will be reviewed later in Chapter 5 and in Appendix A when justifying the behaviour of the fluids used in the experimental setup.

2.2 Optical Theory

2.2.1 Total Internal Reflection

The refractive index is a measure of the phase velocity of light within a medium. The incident light interacts with the electromagnetic field generated by the charged particles within the media. It is given by:

$$n = \frac{c}{v_{phase}} \quad (2.5)$$

Total internal reflection (TIR) occurs when the angle of refracted light becomes $\frac{\pi}{2}$ from the normal. This will be exploited to confine the light into the device. It will occur when the incident light is at an angle greater than the critical angle (obtained via Snell's law):

$$\sin(\theta_{critical}) = \frac{n_2}{n_1} \quad (2.6)$$

where n_2 is the refractive index of the medium in which the refraction occurs. As this quantity must be less than one, it is clear that $n_2 < n_1$ for this relation to hold. The refractive index of a material is dependent on the wavelength of light used[10]. Refractive indices given in this report are quoted as those measured at 488 nm.

2.2.2 Fluorescence

Fluorescence arises from the excitation of orbital electrons within a molecule. These molecules are called fluorophores.

A photon is emitted as the fluorophore relaxes to its ground state. Often, this photon will be of a longer wavelength as some of the excitation energy is dissipated as heat.

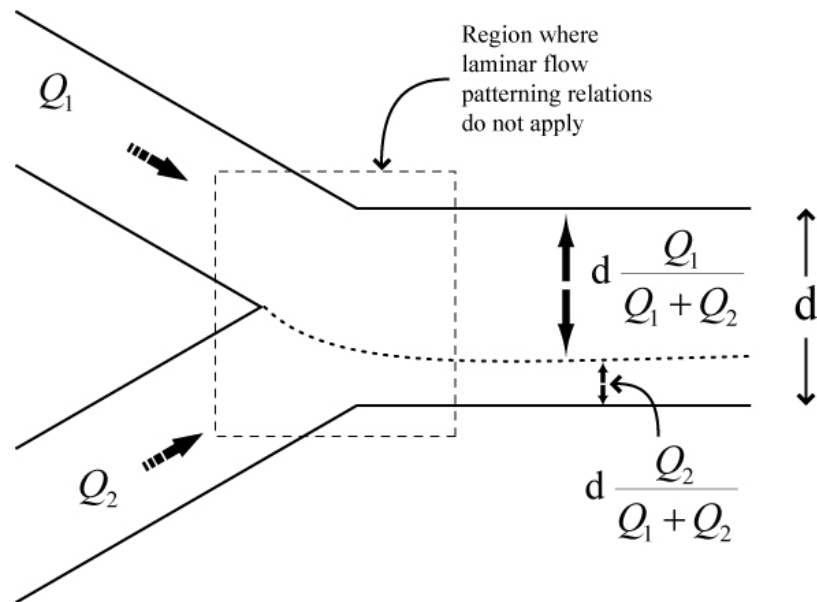


Figure 2.1: LFP with two fluid inputs[6].

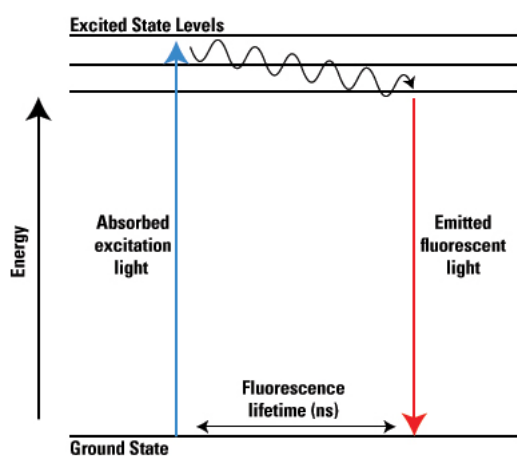


Figure 2.2: A typical fluorescence process[11].

Chapter 3

Method

In this chapter, the design of the devices will be briefly commented upon. The fabrication procedure, the procedure for infusing the devices with fluids, and the optical setup will also be elaborated upon.

3.1 Design

Design was motivated by testing different aspects of the components of an L^2 waveguide in existing devices. For example, it was discovered that the channels bringing the cladding to the main channel, as well as the resistor for the core liquid, obscured the placement of an optical fibre directly behind the waveguide channel. As such, the resistor was moved out of the way, and the cladding channels were bent around the waveguide channel. Fig. 3.1 shows the original design of the device compared to the repurposed device. Device 3.1(a) was selected for modification as it already had the nozzle necessary for LFP. The dimensions of the devices are given in Table 3.1.

In Chapter 5, some recommendations will be presented on future designs of these devices.

Channel	Width/ μm
Core	300
Cladding	200
Main	500

Table 3.1: Dimensions of the channels used within the devices.

The masks used for lithography were designed in AutoCAD, and based upon designs provided by Kadi Liis Saar. The films were then printed by Micro-Litho (<http://www.microlitho.co.uk/>).

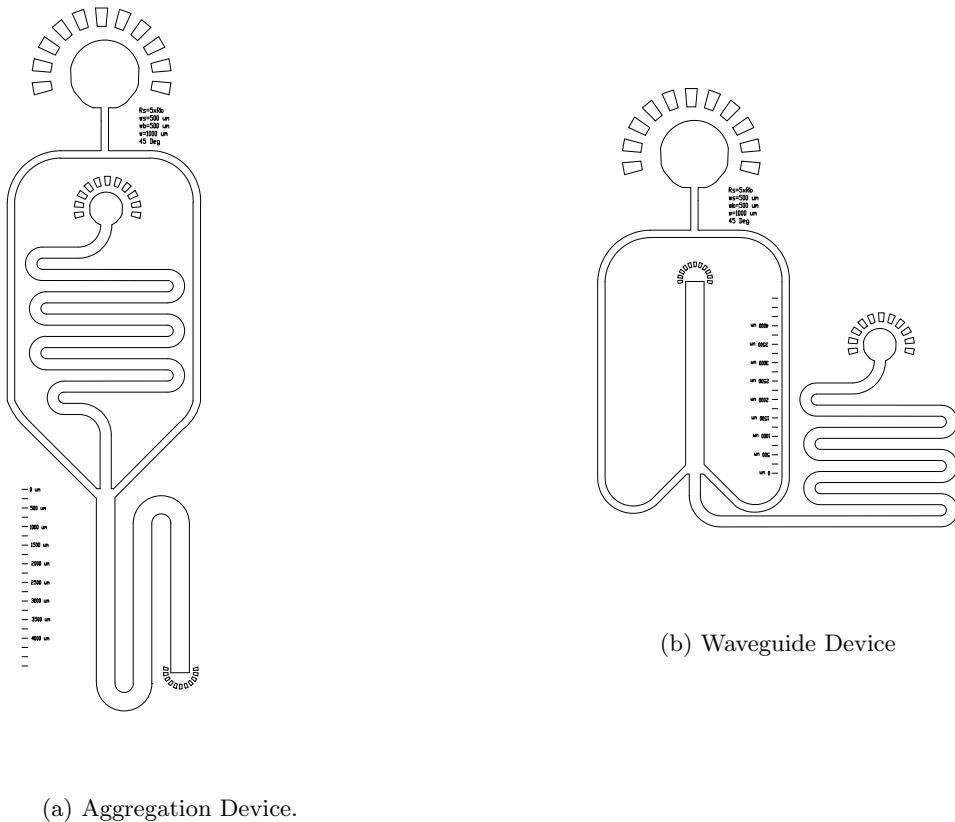


Figure 3.1: A comparison of the devices used. Device (a) was initially used to test the flow between the core and cladding liquids. To provide room for the optical fibre from behind the nozzle, the inner resistor was moved to the side. The cladding channels were moved around the main channel so that only one inlet was required for the cladding.

3.2 Fabrication

3.2.1 Lithography

A process called soft lithography was used to produce the devices. The basical principal behind this process is shown in Fig. 3.2.

A silicon wafer was used as the substrate. It was cleaned using N_2 . The photoresist SU-8 was supplied by Microchem. Approximately 2 ml of SU-8 was applied to the silicon wafer and a spin coater was used to spread it over the wafer with the desired thickness. SU3050 was used for the 50 μm devices. SU3025 was used for the 25 μm devices. They were spun at 500 rpm for 10 seconds at an acceleration of 100 $\text{rpm}\cdot\text{s}^{-1}$ and at 3000 rpm for 30 seconds at an acceleration of 300 $\text{rpm}\cdot\text{s}^{-1}$ in accordance with the SU-8 datasheet recommendations[12].

The wafers were then baked on a hotplate at 96 °C for 12 minutes. After this, a mask was placed on top of the wafer and a glass cover was placed on top. This was supported on a stage and placed underneath a UV source, where the wafers were exposed for 15 seconds at an intensity of 250 mJ/cm^2 . A post-exposure bake on the hotplate lasting 5 minutes was performed. The unexposed SU-8 was removed by development in Propylene glycol monomethyl ether acetate (PGMEA, Sigma Aldrich) for 8 minutes. Once developed, the wafers were washed with Isopropyl Alcohol (IPA) and dried with N_2 .

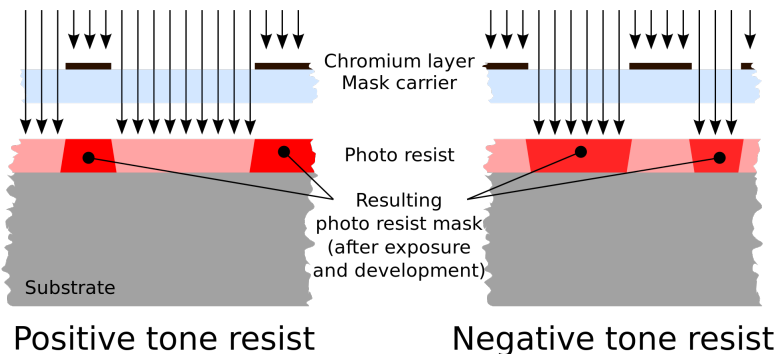


Figure 3.2: A schematic of the photo resist process[13]. This project used negative-tone resist and a plastic film as the mask.

3.2.2 PDMS

Polydimethylsiloxane (PDMS) is the material of choice to fabricate microfluidic devices from. It is transparent at optical frequencies. It has low autofluorescence, which reduces the background noise in measurements.

A combination of 1:10 curing agent to elastomer mixture (Sylgard 184 PDMS Elastomer kit) was used. It was mixed thoroughly before pouring onto the master. After pouring, bubbles were removed by dessication for 30-45 minutes.

For 33g of the curing agent/elastomer mix, the devices were baked at 65 °C inside an oven for 3 hours. The duration was reduced linearly for smaller amounts, for example, when making thinner devices. Devices were then cut out using a scalpel. Once the devices were baked and cut out, the inlet holes were punched out and cleared using N_2 .

Black PDMS was used to reduce noise from external light sources and to improve measurements within the device by reducing reflections at the external boundaries of the transparent PDMS[14]. This is shown in Fig. 3.3. Totally encasing the device in black PDMS was ruled out as it would obstruct observing the channels.

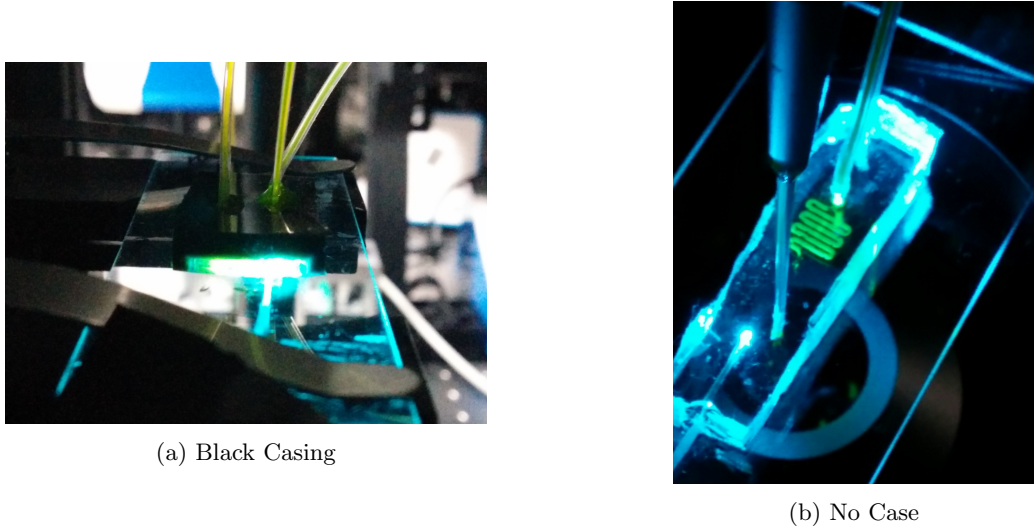


Figure 3.3: Devices with different casing being illuminated with an optical fibre.

Carbon Nanoparticles were added to PDMS which had been prepared in the described manner. For 25g of curing agent/elastomer mix, a large spatula worth of nanoparticles were added and mixed into the PDMS. The resulting mixture was centrifuged for 5 minutes at 4000 rpm.

3.2.3 Placement of Optical Fibre

A multimode optical fibre (ThorLabs FT400EMT) with numerical aperture 0.39 and core diameter 400 μm was used.

Due to space constraints, both on the master and within the oven, the following technique was developed to create cavities in the PDMS with the dimensions of the optical fibre used.

Optical Fibres were prepared by stripping the jacket to expose the cladding (Fig. 3.4a, Fig. 3.4b). The tip was cut using a ruby blade. Afterwards, the head of the fibre was cut off. Part of the jacket was retained in order to provide grip later on (Fig. 3.4c).

The tips were placed on the silicon master (Fig. 3.4d, Fig. 3.6) and they were aligned behind the nozzles of the devices. Blu-Tack was used to hold them in place. This helped direct the aperture of the fibre towards the SU-8 ridges, improving alignment with the channels. Originally, Magic Tape was used, but

it was found to be easier to realign the tips with Blu-Tack application.

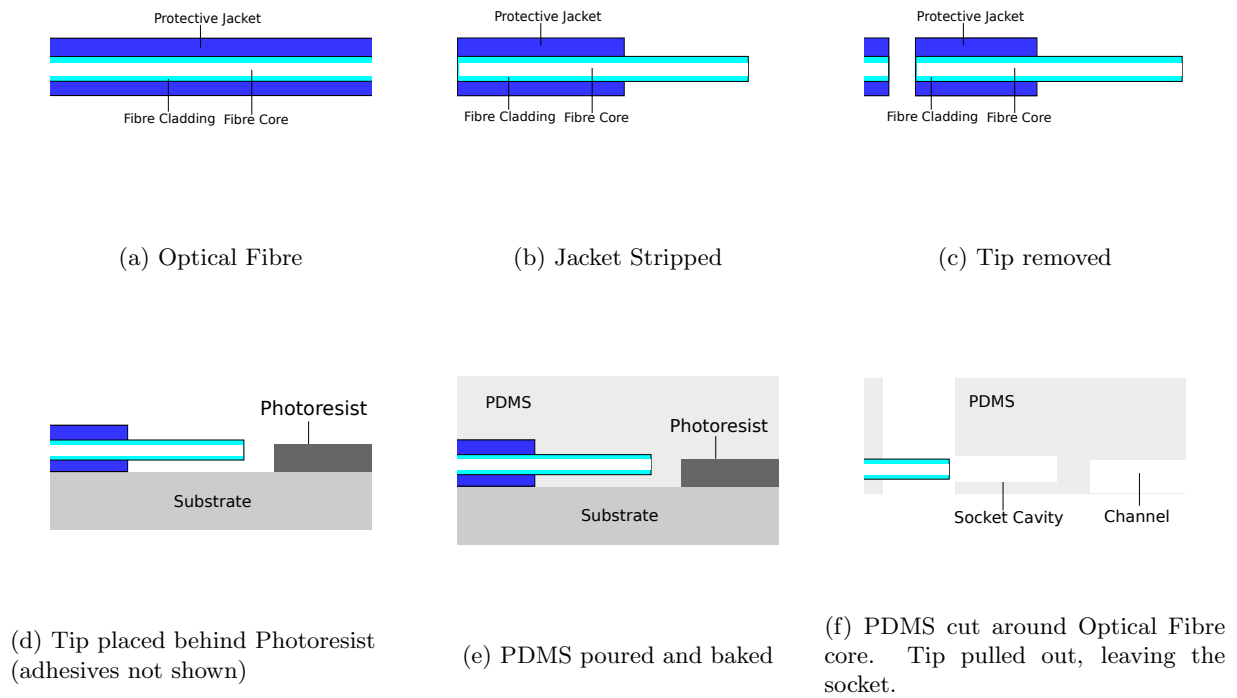


Figure 3.4: Outline of the process used to create the socket (not to scale).

PDMS was poured onto the master, and baked with the fibres inside (Fig. 3.4e). After cutting out the devices, the tips were removed by cutting around the cross section of the cladding and pulling on the jacket (or the PDMS surrounding the jacket)(Fig. 3.4f). This left a circular socket for an optical fibre to be inserted. This is shown in Fig. 3.5. The tips were recovered and reused to create several devices. Multiple sockets for one device can be created by placing tips around the device.

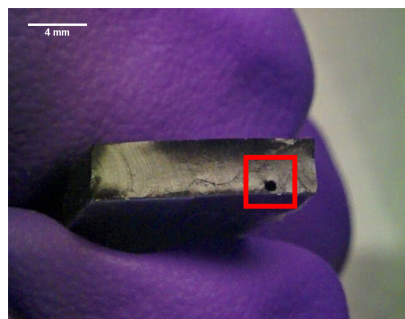


Figure 3.5: An optical fibre socket in a device.

This process was advantageous because it reduced the space requirements needed to bake the devices; allowed for the production of multiple devices at once; allowed for one optical fibre to be used with many devices; and offered finer control over optical fibre placement than piercing a device with an optical fibre. Previous attempts involved placing the entire optical fibre inside the oven while the device was baking and they were not intended to be removed.

The sockets have their drawbacks. Careless insertion can pierce the channel, causing fluids to leak out. Likewise, the socket can be widened by incorrectly inserting the fibre. Switching between different sizes of optical fibre can lead to bad alignment. The tip of an optical fibre can snap off inside the cavity, which might not be removable.

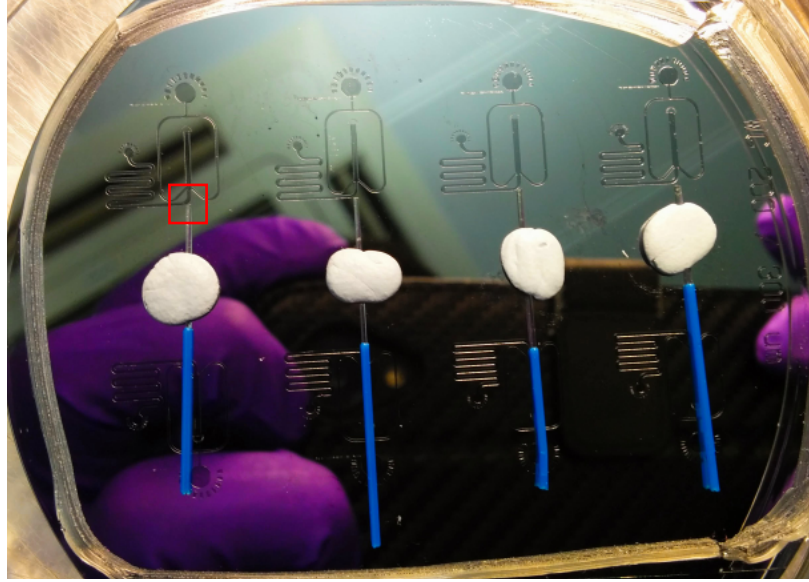


Figure 3.6: Optical fibre tips placed against the device master. The alignment of devices could be improved in order to maximise the number of devices which can be made in one sitting. To show specifically where the tip is located, a red box has been drawn.

3.2.4 Cleaning

During the testing of devices, it was noted that the two phase flow was not parallel and suffered from a series of kinks and bends throughout the channel. In some cases, it was observed that the Fluorinert/Water would flow around dirt particles in the channel. To reduce the impact of these imperfections, the devices were cleaned.

Before bonding, dirt was removed by applying Magic Tape on the sides of the devices containing the channels. The tape was removed and reapplied repeatedly for approximately 20 seconds.

Multiple devices (maximum: 4) were added to a Falcon tube containing 30 ml of IPA. They were then sonicated at room temperature in an ultrasonic bath. The devices were removed from the tube using a cleaned pair of tweezers, and dried using N_2 .

IPA wipes (Kimtech, 70% IPA) were used to clean the glass slides for bonding. These were also dried using N_2 .

3.2.5 Plasma Treatment

Plasma treatment was used for two purposes: bonding the devices to a substrate, and treating the devices to make them hydrophilic.

An oxygen plasma was used to create several oxygen bonds on the devices and on the glass. The formation of Hydroxyl (-OH) groups on the PDMS and glass increases the hydrophilicity of the devices[15]. This was performed in order to minimize the surface energies at the fluid-solid interfaces.

In both cases, a Diener 'Femto' plasma treatment device was used. The devices were placed inside and the plasma treater was sealed. The pressure inside the container was 4 millibar. Oxygen was allowed to fill the container for two minutes before treatment began. The maximum power available was approximately 1450 W.

The settings used for two different cases are given in Table 3.2.

	Time/s	Power (% of Max.)	Oven Pre-bake
Bonding	15	40	No Bake
Hydrophilic Treatment	500	80	10 minute bake @ 65 °C

Table 3.2: Conditions used for bonding and hydrophilic treatment inside the plasma device.

The devices were bonded to Thermo Scientific Menzel-Gläser (BS7011/2) slides. The hydrophilic properties of treated PDMS vary over time[16]. In order to reduce the effects of changes in surface properties of PDMS, they were immediately filled with deionized water after treatment. PDMS is chemically resistant to deionized water, and as a result does not experience significant hydration.[17].

3.3 Infusion

3.3.1 Setup

neMESYS pumps were used in order to infuse liquids into the devices. The pumps were controlled using the neMESYS software. Syringes (HSW Norminjekt 1 ml) were used to hold the liquids. Large air bubbles were removed by tapping the syringes and pushing them out with the plunger. Needle tips (Agani 25Gx1") were attached to the syringes, and smaller air bubbles were pushed out in the same way. Polythene tubing (Smiths Portex 800/100/120) was attached to the end. The tubing was cut at a 45 degree angle at one end in order to help insertion into the devices. A pipette tip was inserted into the outlets.

3.3.2 Fluids Used

The properties of the fluids used are highlighted in Table 3.3.

Fluorinert FC-40 is a perfluorinated oil, manufactured by 3M. Fluorescein (2mg/ml) was used as the fluorescent material. It is often used to label and track cells in fluorescence microscopy. Its fluorescence spectrum is given in Fig. 3.7.

The addition of Fluorescein may change the refractive index of the water[25]. The refractive index contrast between FC-40 and Water is 0.044. A typical optical fibre will have a cladding refractive

Fluid	Density/gcm ⁻³	Viscosity/cSt	Surface Tension/mN·m ⁻¹	Refractive Index (488nm)
Water	1.000	0.89	72.8 (air)	1.335
FC-40	1.855	2.2	52.1 (water)	1.290
Methanol	0.791	0.69	22.95 (water)	1.331

Table 3.3: Properties of the fluids used in the experiment[18][19][20][21]. Methanol will mix with water so the surface properties will vary over the length of diffusion. Data provided in range 20-25 °C . Surface tensions given as those with their surrounding media[22][23][24].

index of approximately 1.4440 and a core index of 1.4475[26]. The difference here is 0.0035, which is not a large difference. Therefore, the difference due to the addition of Fluorescein was not measured as it was considered that the change would be insignificant compared to the difference in refractive indicies present, and those of an actual optical fibre.

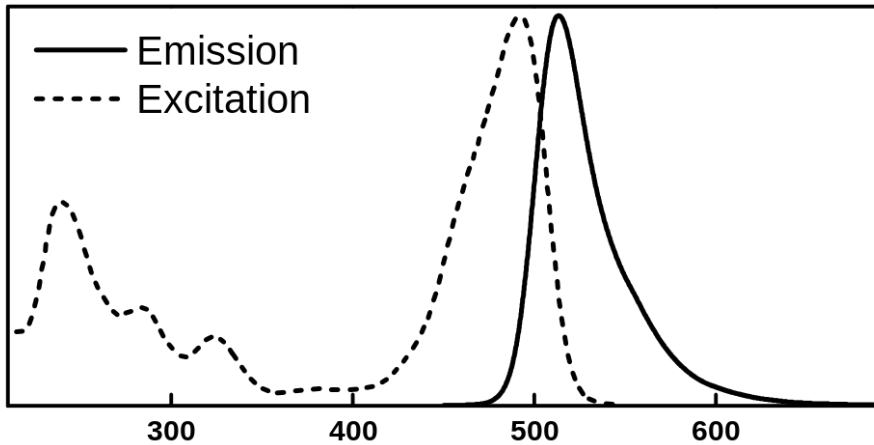


Figure 3.7: Fluorescein emission spectrum[27]. The x-axis represents the wavelength (in nm) of light. Peak excitation occurs at around 480 nm.

3.3.3 Procedure

Flow measurements were originally conducted within the aggregation device. Flow rates were explored by varying the flow rates by increments of $50 \mu\text{lh}^{-1}$.

For optical measurements, devices were flushed with cladding liquid before use. This was performed in order to remove any remaining fluorescent material present in the channels, which could potentially add noise to the measurement. The flow rate of the core and cladding syringes was held at $250 \mu\text{lh}^{-1}$. as this formed a stable flow pattern which started quickly. The width of the flow was also wide enough to make clear measurements. Images were taken using the optical setup described in Section 3.4.

For the same reason as outlined in Section 3.2.5, the devices were filled with water after use.

3.4 Optical Setup

3.4.1 Lab Microscope

Flow measurements were conducted on a lab microscope. Light was incident on the devices from above. The channels were then focused upon. A magnification of 10x was used for the majority of measurements.

3.4.2 Laser Fluorescence Setup

A fluorescence microscope was built to measure the coupling of light to the devices. An optical bench was used to mount the equipment. This reduced vibration from the surroundings.

The devices were supported on a stage, which provided movement in the xyz directions. An objective lens (Nikon Plan Fluor) of numerical aperture 0.3 and magnification 10x was placed underneath the observation bay. A mirror reflected this light into a dichroic mirror which passed the light into an emission filter (at 488 nm) in order to remove the laser light from the measurements. A UV LED was connected to the dichroic mirror, which allowed for illumination of the devices through the objective lens. The beam splitter was later removed, and the filter replaced with a 488 nm line filter to check the extent of laser light leaking from the device. After this stage, light was passed into a tube lens (ThorLabs SM2A20) with focal length 200 mm. This focused light into a camera (QImaging optiMOS) and the images were observed on a computer. To achieve this, the tube lens was placed 200 mm from the camera sensor. The camera sensor was 17.5 mm inside from the camera casing; this was accounted for. A lens was placed on the outside of the camera. Tubing was used to shield from external light sources. Mounts were securely tightened to prevent error arising from unintentional displacement or vibration.

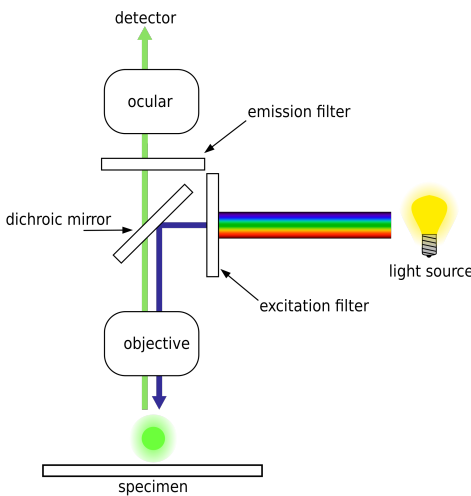


Figure 3.8: A schematic of a typical fluorescence microscopy setup[28]. This is what was built for the experiment.

A laser (Obis No. 1185053) of wavelength 488 nm was used as the light source. It had the capacity to go up to 50 mW, however this was limited to 30 mW in the interest of safety and because it was not

felt that going beyond this power was necessary. An optical fibre was plugged into a connector which was then screwed onto a mount. The connector was aligned with the laser light by adjusting the mount. The laser was then switched off. The glass slides holding the devices were placed on the stage. UV light incident from underneath the devices was used to focus on the channels. An index matching liquid (Olympus Immersion Oil Type-F, $n = 1.518$) was applied to the tip of the optical fibre. This was then inserted into the socket. The lights within the room were switched off and the computer screen was pointed away from the devices in order to reduce external noise.

3.4.3 Laser Measurements

Images were taken close to the nozzle where the fluids met and further down the channel, so as to determine the change in intensity down the channel. Exposure times of 10ms and 1000ms were used.

Recording down the channel was also used with the aim of reducing the effects of light coupled without TIR, either directly or via reflections from PDMS interfaces. The position markers, as shown in Fig. 3.1, were often damaged during fabrication, or were not visible due to the black PDMS. This meant that the distance traversed was not established.

The devices were filled with cladding liquid in order to demonstrate that the laser was not fluorescing the cladding.

Once the images were recorded, the channels were highlighted in the images and intensity histograms were produced using software.

3.4.4 Software

Measurements were taken using Micro-Manager (<https://micro-manager.org/>) software.

The laser power was controlled using CoherentSource (<http://lasers.coherent.com/lasers/obis-software>).

Images were processed using ImageJ (<https://imagej.nih.gov/ij/>) software.

Chapter 4

Results

4.1 Fluid Measurements

4.1.1 Two Phase Flow

Stable two phase flow between FC-40 and Water was observed. Two different flow regimes were observed. In hydrophobic devices, LFP was observed but only beyond the $500 \mu\text{lh}^{-1}$ range (for both fluids). Below this range, the LFP was unstable. Slug formation became dominant. A comparison is provided in Fig. 4.1. Additionally, some laminar flow was established further downstream after the initial stream disintegrated. Due to the difficulty of calculating the flow velocities in these regions, they were not considered. The flow profiles for varying inlet flow rates are compared for hydrophilic devices in Fig. 4.3 and in Fig. 4.2 for hydrophobic devices. Scale bars in all images correspond to a length of $250 \mu\text{m}$.

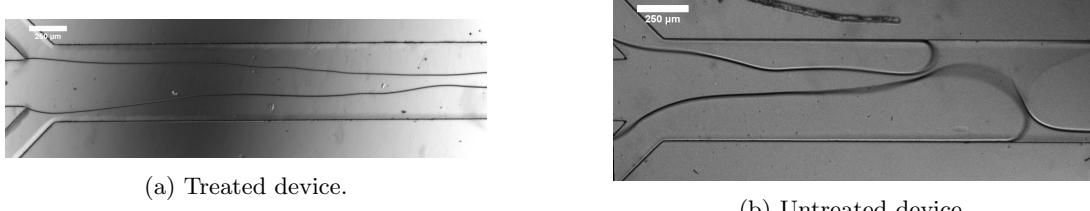


Figure 4.1: Comparison of effect of plasma treatment on devices. The device in (a) is hydrophilic and the laminar flow is established. It is more favourable for closed volume 'slugs' to form in the hydrophobic case shown in (b). The flow rates at the inlets for both liquids was $500 \mu\text{lh}^{-1}$.

The widths of the inner and outer streams were compared with Eqn. 2.3. It was found that these results did not conform to the ratios predicted. An attempt to explain this is given in the next chapter.

4.1.2 Cleanliness

Devices which were given sonication cleaning were compared with those which were bonded without cleaning. Parallel flow was better established within cleaner devices, although not always perfectly so.

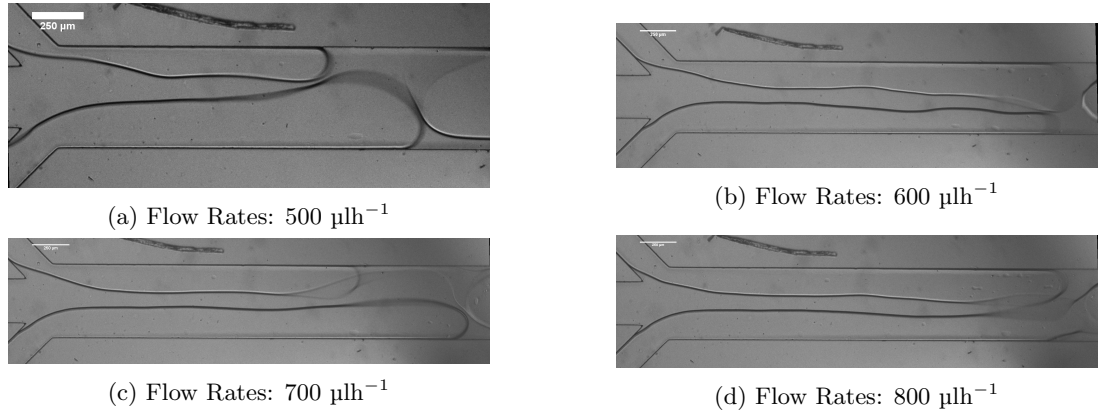


Figure 4.2: Flow inside non-sonicated, hydrophobic devices. Flow rates are given as those at the inlets. The inertial forces below the $500 \mu\text{l h}^{-1}$ range become increasingly insufficient to stabilise the flow. The length scale at which droplets was noted to level off at flow rates close to $1000 \mu\text{l h}^{-1}$.

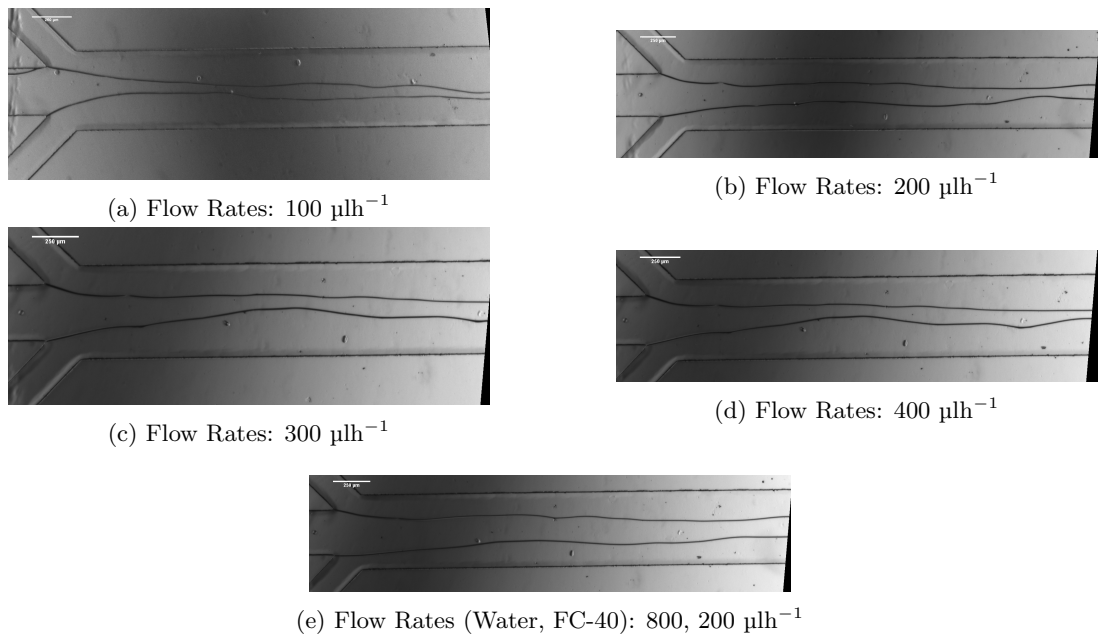


Figure 4.3: Flow inside non-sonicated, hydrophilic devices. Flow rates are given as those at the inlets. It is clear that a lack of cleaning give sub-optimal flow profiles.

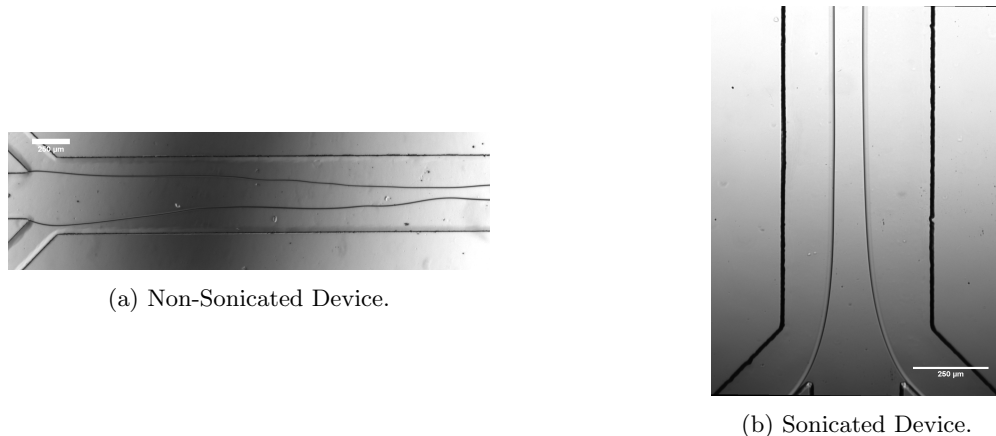


Figure 4.4: Comparison of flows inside devices which have and have not been given sonication in order to clean them. The reduction of attraction sites inside the clean device improves the form of the flow. The flow rates at the inlets for both fluids in these images was $500 \text{ } \mu\text{l h}^{-1}$

These results recommend the use of hydrophilic, sonicated devices for testing if FC-40 is to be used.

4.1.3 Methanol Flow

Devices using methanol as the cladding liquid were also measured. LFP was established immediately regardless of treatment or cleanliness.

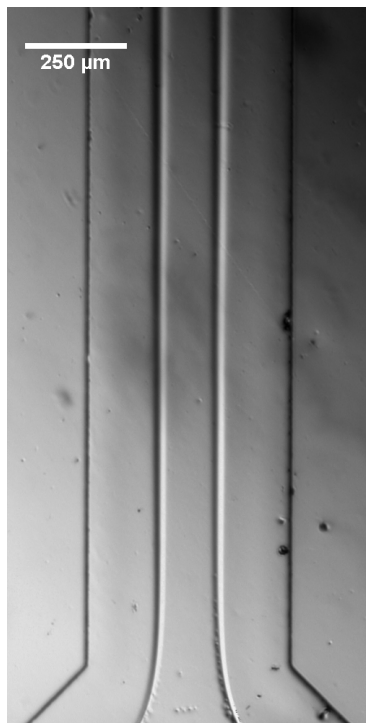


Figure 4.5: LFP established inside a device using methanol. Water, Methanol flow rates: $(400, 1600) \text{ } \mu\text{l h}^{-1}$. Surface energy effects are greatly reduced, contributing to the ease at which this flow can be established.

4.2 Optical Measurements

Devices encased in the black PDMS casing were initially checked with the UV backlight. Results from two separate devices are presented for FC-40 cladding. In the second device, an exposure time of 10ms was used and was measured at three points (nozzle, channel, outlet). A third device was used to observe Methanol as a cladding liquid. In all results shown in this section, flow rates at the inlets were $250 \text{ } \mu\text{l h}^{-1}$. Intensity histogram plots are presented. Log-10 comparisons are shown in order to highlight the broad range of intensities.

4.2.1 Device A

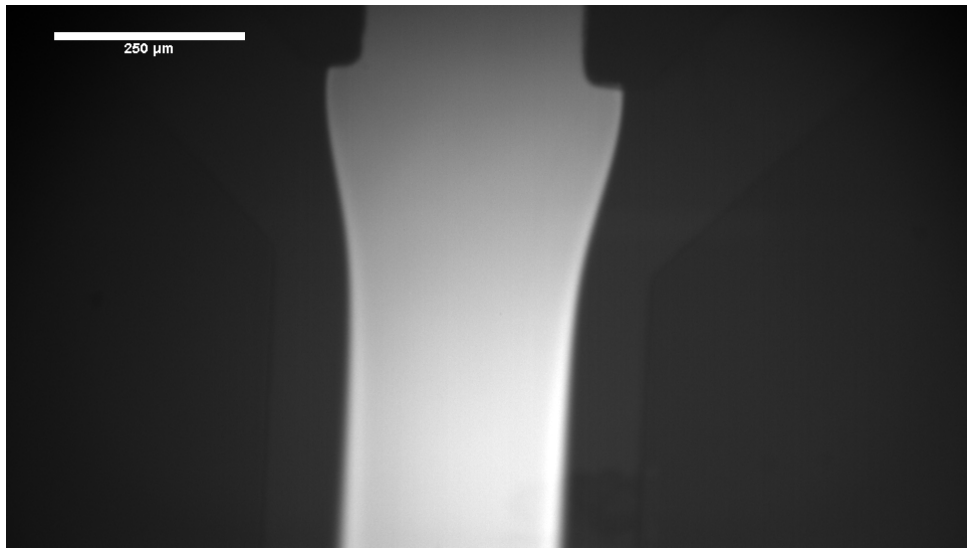


Figure 4.6: Nozzle illuminated with UV LED

To measure the intensities accurately, an area of Fig. 4.7a was selected to exclude the area where light was scattering from the PDMS.

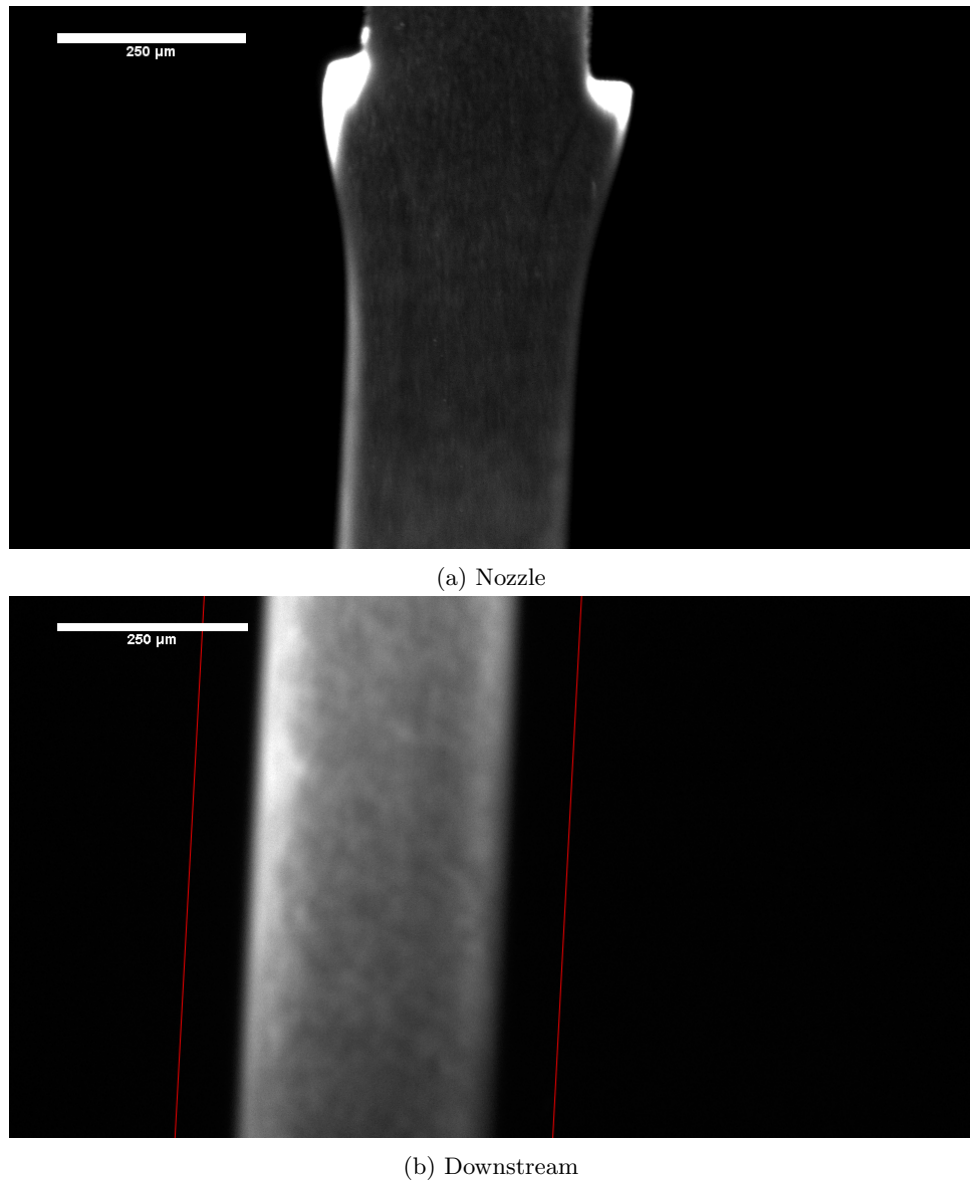


Figure 4.7: Images of fluorescence using FC-40 as the cladding liquid. The laser power was 20mW and images were taken over an exposure time of 1000ms. In (a), the formation of LFP can be observed by the narrowing of the stream. The boundaries of the channel have been highlighted in red in (b).

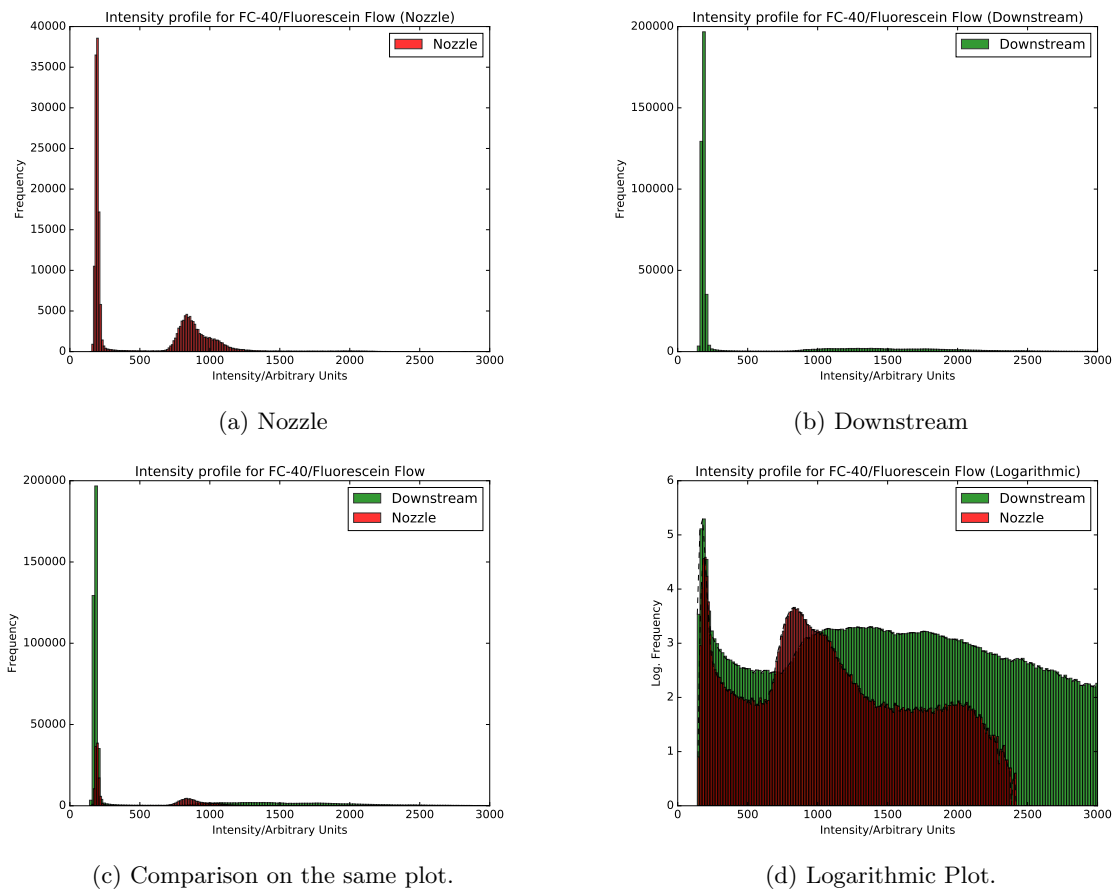


Figure 4.8: Intensity profiles comparing the two images from Device A in Fig. 4.7.

4.2.2 Device B

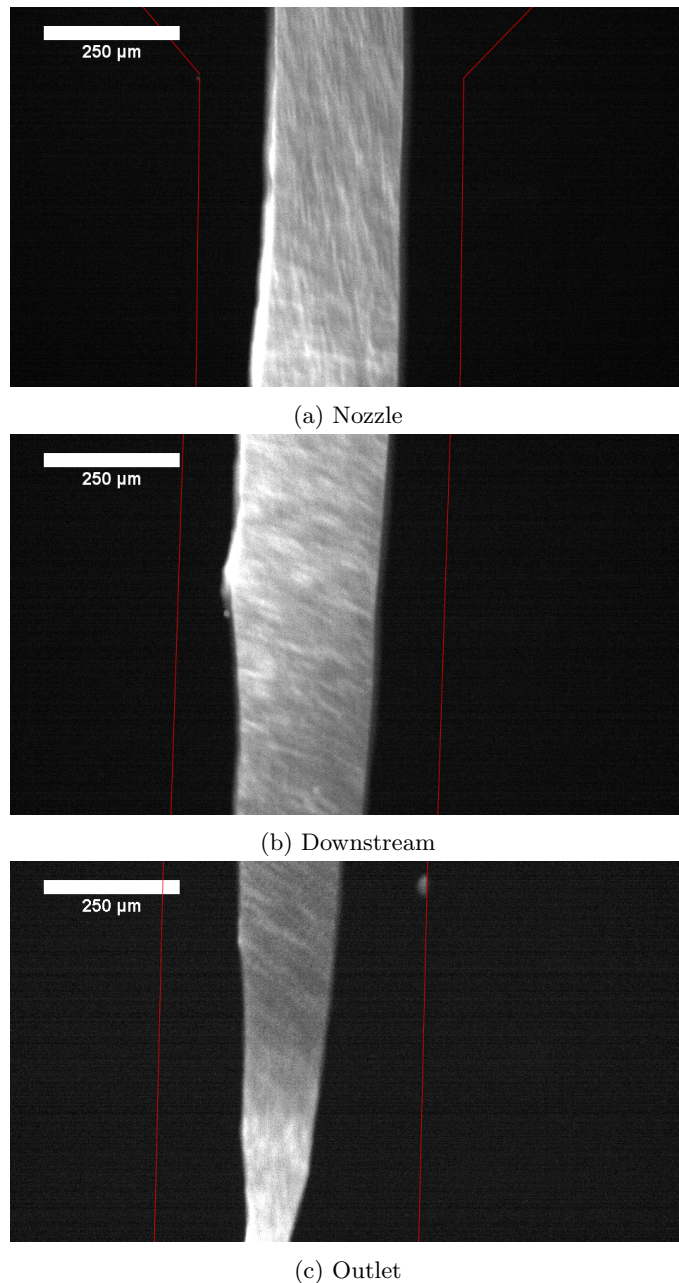


Figure 4.9: Images of fluorescence using FC-40 as the cladding liquid. The laser power was 20mW and images were taken over an exposure time of 10ms. The flow profile was not as uniform as that in Device A. The coarse pattern is not thought to be from reflected light rays but a pattern arising due to the core fluid. The boundaries of the channels have been marked in red.

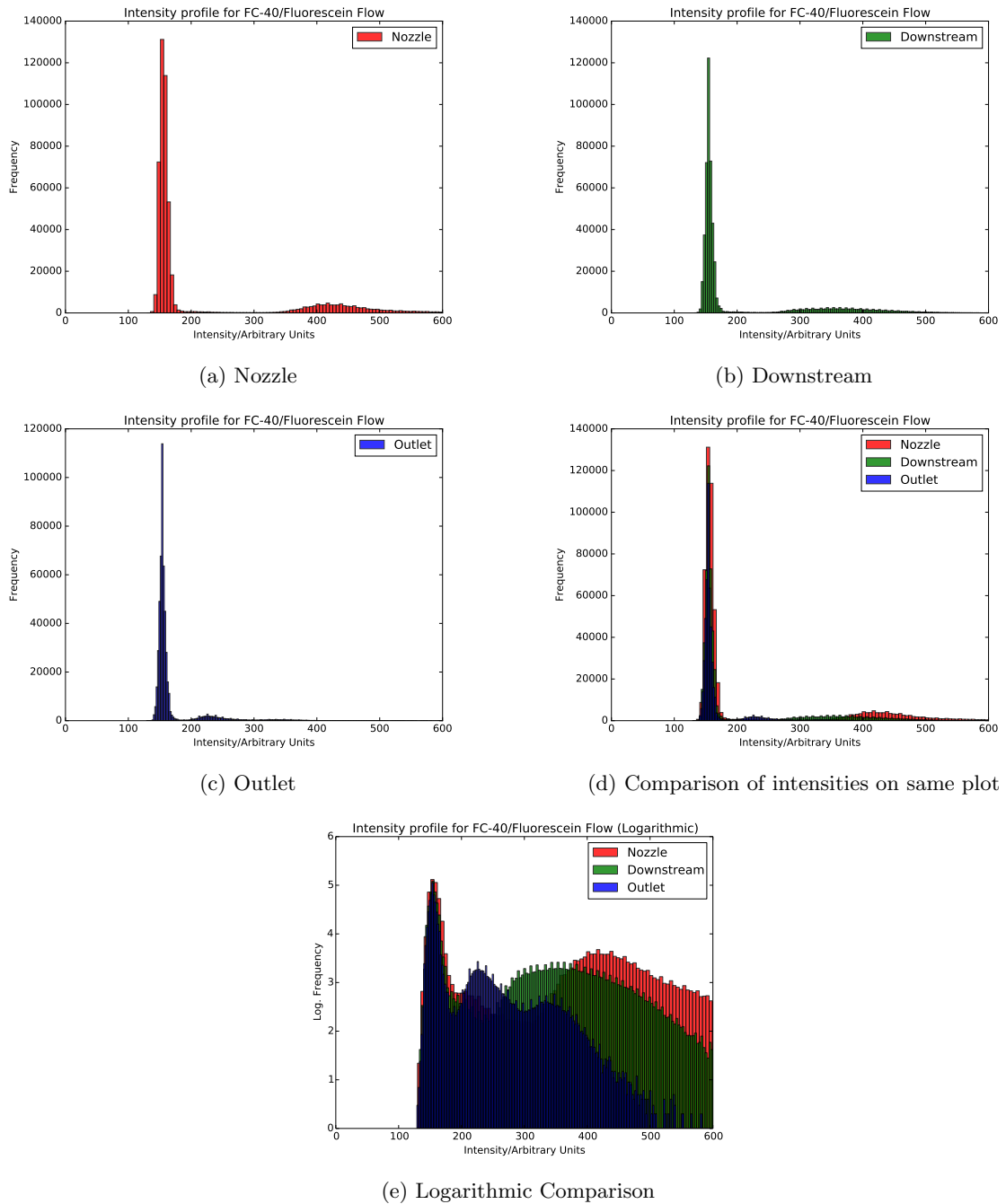


Figure 4.10: Intensity profiles comparing the two images from Device B in Fig. 4.9

4.2.3 Methanol

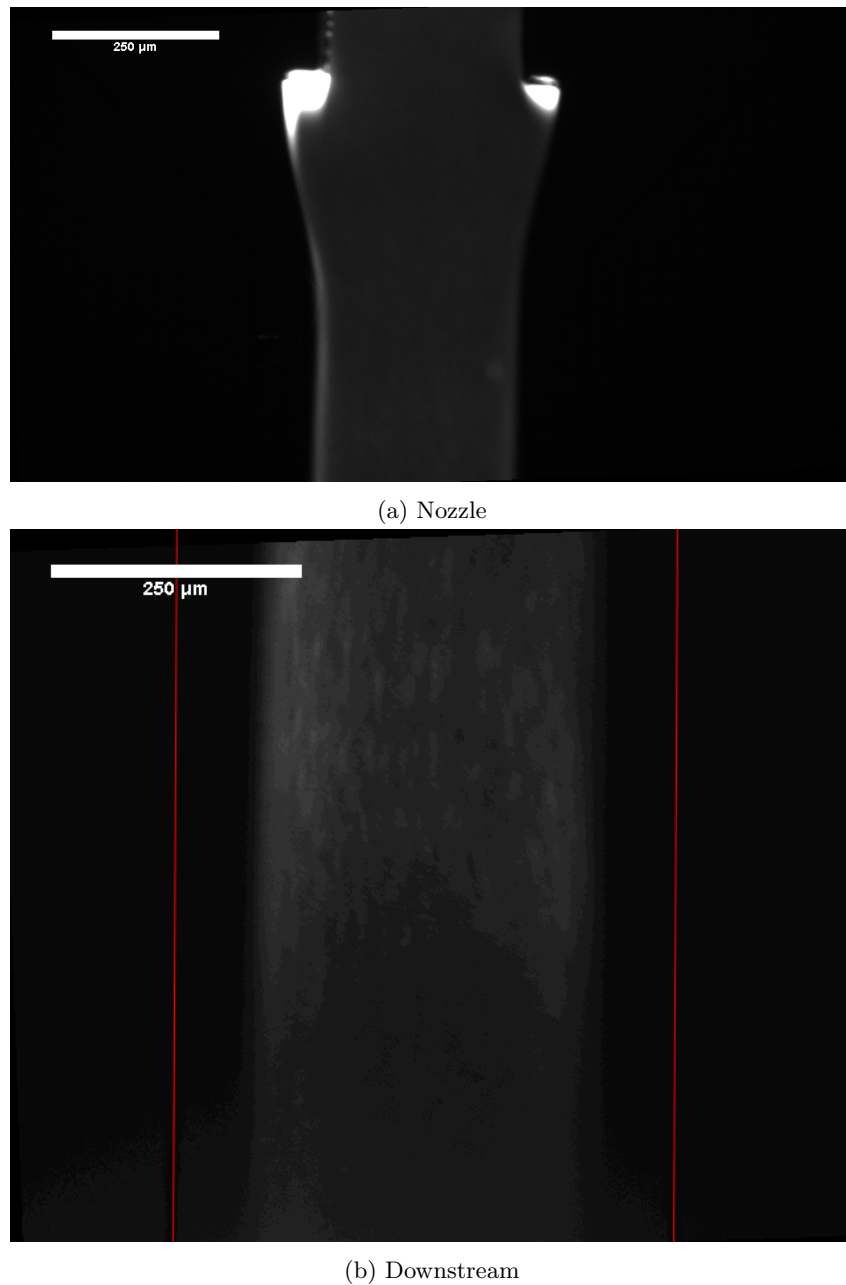


Figure 4.11: Images of fluorescence using Methanol as the cladding liquid. The laser power was 20mW and images were taken with an exposure time of 1000ms. To measure the intensities, an area of (a) was selected to exclude the area where light was scattering from the PDMS edges of the nozzle. In (b) the outline of the channel has been marked in red.

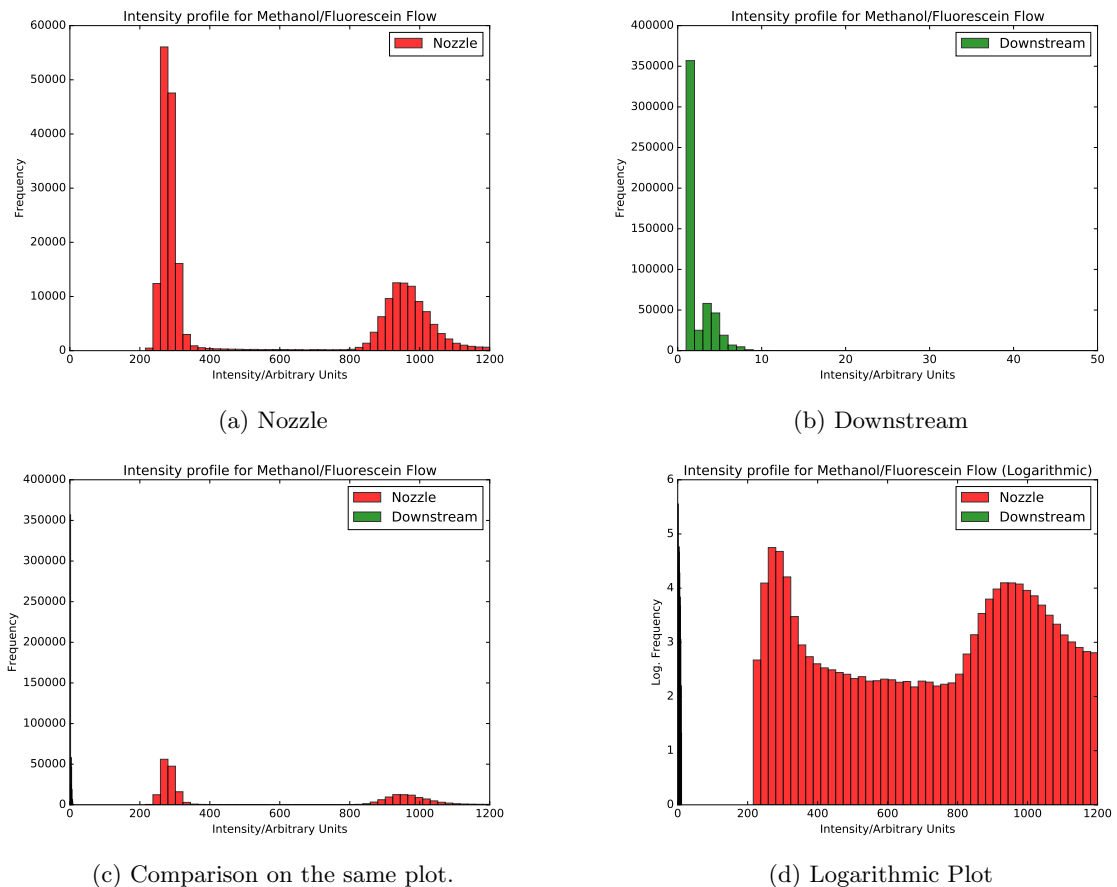


Figure 4.12: Intensity profiles comparing the two images of the Methanol device in Fig. 4.11. Most of the second image is significantly darker compared to the first.

Chapter 5

Discussion

5.1 Two Phase Flow

In order to achieve stable flow at low flow velocities, it is essential to treat the devices with the plasma.

As outlined in Section 2.1.4, the fluid systems tend to arrange themselves in order to minimise their surface energies. Typical analysis of the Rayleigh-Plateau instability models columns of liquid which are cylindrically symmetric. This symmetry is not present inside the microfluidic devices used. To motivate the investigation of two phase flow inside microfluidic devices, the droplet formation argument from Section 2.1.4 was adapted to (Appendix A):

$$R > \frac{3\gamma_f}{\frac{\gamma_g + \gamma_p}{h} + \frac{2\gamma_f}{w_c}} \quad (5.1)$$

One can consider setting the radius of such a droplet to be comparable to the height of the channel. This would prevent the formation of spherical droplets inside the channel. The formation of slugs as the product of the instabilities present is consistent with this analysis as spherical droplets are not the only geometry available.

The formation of -OH groups from the plasma treatment allows for control of these fluid-solid surface energies. This was exploited in the fabrication of the final devices used.

The height of the channels was also considered. Initially, devices were built at 25 μm , 50 μm , and 100 μm . LFP was not established in 100 μm hydrophilic devices. 50 μm was selected in order to maximise the overlap between the optical fibre output and the channel.

Hydrophobic devices can be used, but require flow rates greater than 500 $\mu\text{l h}^{-1}$. This could pose issues for experiments which are interested in tracking particles. It would not be practical to use untreated devices if the core liquid were to be utilised in another microfluidic component later on inside the device.

The results in Fig. 4.4 highlight the importance of clean devices, as discussed in Section 3.2.4. A non-

uniform flow profile would limit the TIR performance inside the device as the light is more likely to be incident on an interface at an angle less than the critical angle. Cleanliness is essential to reduce error when performing fluorescence microscopy.

The widths of the fluid layers in the channels were inconsistent with those predicted by Eqn. 2.3. Cleaner devices could be used in order to obtain clearer measurements. However, data obtained from clean devices also corroborated this observation. This could be due to fabrication errors of the inlet junction, or from flow properties not considered within the device (e.g. capacitance). This was not detrimental to the function of the final devices.

The results found proved instrumental in proceeding to the next stage of constructing an optofluidic device.

5.2 Optical Measurements

An optofluidic device was successfully built. However, there are a number of technical and experimental challenges which must be considered.

Fluorescence of a fluorophore is independent of the intensity of light. It can be established by even weak sources of light, provided that the photon energies are correct. There are many ways of light entering the channel. As such, it is difficult to determine the amount of fluorescence caused by TIR modes. The ways in which light can enter the channel are listed below:

1. TIR coupling of light into the channel from the optical fibre.
2. Coupling of the light into the channel at such an angle that TIR does not occur, or that the light travels far without interacting with any fluid interfaces (Direct Illumination).
3. Reflection from the fluid-solid (PDMS, glass) layers.
4. Reflection from the solid-air layers.
5. External light from the environment entering the device.

As outlined in Chapter 3, the light inside the room was considered and minimised during measurement. Sometimes the computer monitor had to be tilted towards the setup in order to use the software to record images, this did not significantly impact measurements. Reflection from the solid surfaces was expected to be low. The black PDMS case reduced this effect further[14], as well as acting as a final shield against external light entering from above.

The optical fibre was coupled behind the channel, parallel to the axis of flow. As such, it was thought that fluorescence was primarily excited by process 2. The results in Section 4.2 seem to support this, particularly in Fig. 4.10d. In the intensity profiles, there are large peaks of relatively low intensity light, regardless of channel position. While light was coupled to the channel, it does not seem that TIR was observed inside the devices. TIR light can also zig-zag out of the device. These modes would not be

propagated over a long distance. Typically, a lens is used to couple laser light to an optical fibre. In the devices presented, no such lens is used. As a result, light is transmitted over a cone of light, further reducing the coupling efficiency to the channel.

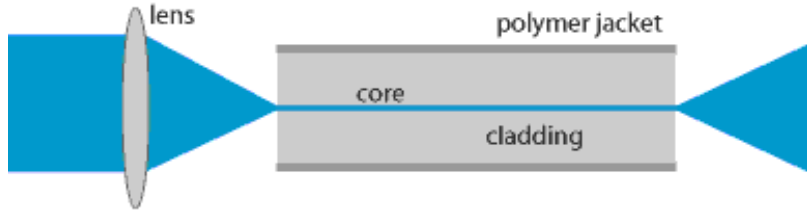


Figure 5.1: To couple laser light to an optical fibre, lenses are used to focus the light on to the fibre[26].

As demonstrated in Fig.4.12, light coupled via TIR has not been observed in the case of Methanol either.

5.3 Further Work

Significant improvements to the coupling efficiency could be made. This could be done by investigating with single mode fibres, which have a diameter closer in size to the wavelength of light used as well as the height of the channels.

A simple test of the waveguide properties of these devices would be to construct an entirely carbon black device, with a series of bends in the main channel. This would allow for fluorescence to be detected in regions not directly illuminated by and those behind the plane of the optical fibre aperture. This was attempted with a device like the one shown in Fig. 3.1a, however the devices tested failed to work, and no results were taken. The existing bends in the design would also lead to a lot of losses, in the same way that light can leak from a normal optical fibre when bend. The waveguide device in Fig. 3.1b was designed to allow optical fibres to be coupled without interfering with the inlet channels. As a result, there was little room for a bend which would be sufficiently far removed from the optical fibre's output as to make a reliable measurement. Future designs which rely on an optical fibre socket could add parallel lines to the lithography mask in order to create a ridge which could hold the optical fibre in place without the requirement for Blu-Tack. Lenses can be made within a PDMS environment[29]. It would also be worthwhile investigating if a lens could help focus light onto the channels at the correct angle for TIR.

There are other low refractive index liquids which are immiscible with water. One such liquid is Fluorinert FC-72, which has a refractive index 1.251[30].

Additionally, experiments could be performed where the optical fibre is inserted directly into the channel. This was attempted over the course of the project but was limited by the devices leaking.

Chapter 6

Conclusion

A proof-of-concept liquid core, liquid cladding optofluidic waveguide was designed and tested.

Water ($n = 1.335$) containing Fluorescein (2mg/ml) was used as the core liquid. Fluorinert FC-40 ($n = 1.291$) was used as the cladding liquid. Methanol ($n = 1.331$) was also used as a cladding liquid.

The inherent fluid dynamical instabilities between two immiscible fluids were overcome in order to create the waveguide. This was accomplished by using plasma treatment to create a hydrophilic environment within the device. Additionally, it was noted that the same effect can be achieved without treatment by using high flow velocities (greater than $500 \text{ } \mu\text{l h}^{-1}$).

An optical fibre (core diameter 400 μm , numerical aperture 0.39) was successfully used to couple light into the channel. However, due to the position of the optical fibre relative to the channel, the strength of the effect was unclear. As such, no coupling efficiency is given. A method has been proposed in order to see any TIR coupling inside the devices. It was thought that most of the fluorescence detected was caused by direct illumination of the channel.

The technique developed to create sockets for optical fibres on devices allowed for faster production and testing. These sockets wore with usage and could pierce the channels.

In future, optical fibre coupling could be improved by using thinner fibres, device masters to improve the alignment, as well as lenses built into the devices to focus the light.

Appendices

Appendix A

Adapting Surface Energies

Argument adapted from Tabeling[9]. This motivates the use of hydrophilic treatment in order to reduce the surface tensions γ_p and γ_g to inhibit the formation of droplets within the channel. It does not attempt to prove exactly that it is always possible to form stable LFP between immiscible fluids.

Consider the laminar flow between two immiscible fluids in a microfluidic channel which looks like that shown in Fig. A.1.

The core fluid is in contact with: the cladding fluid, the PDMS, and the glass. The dimensions given are shown in Fig. A.1.

Contact Surface	Contact Area	Surface Tension
Glass	Lw_c	γ_g
PDMS	Lw_c	γ_p
Cladding	$2Lh$	γ_{cl}

Table A.1: Properties which determine the surface energy of the core cuboid.

The volume of the core cuboid is hw_cL .

The surface energy is:

$$\begin{aligned} E_{core} &= \gamma_g Lw_c + \gamma_p Lw_c + 2\gamma_{cl} Lh \\ &= V \left(\frac{\gamma_g + \gamma_p}{h} + \frac{2\gamma_{cl}}{w_c} \right) \end{aligned}$$

A droplet of radius R containing the same volume as the core cuboid has surface energy:

$$E_{drop} = \frac{3\gamma_{cl}V}{R}$$

Thus, a droplet will have a lower energy than the cuboidal column if:

$$R > \frac{3\gamma_{cl}}{\frac{\gamma_g + \gamma_p}{h} + \frac{2\gamma_{cl}}{w_c}}$$

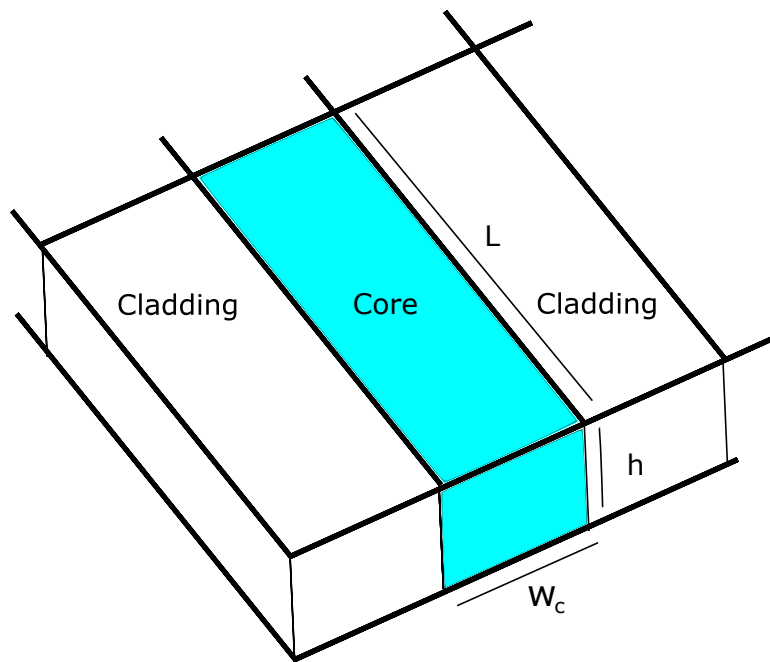


Figure A.1: Diagram of cuboidal column of fluid. Not shown: Contact of the fluids and solid surfaces. In reality, there will be some bending between the fluid interfaces and their contact points with the solid surfaces (Young's Equation).

Thus, there are multiple properties of the microfluidic environment that can be modified to favour laminar flow.

Bibliography

- [1] <http://www.elveflow.com/microfluidic-tutorials/microfluidic-reviews-and-tutorials/the-poly-di-methyl-siloxane-pdms-and-microfluidics/> (Accessed 5/5/2016)
- [2] Sia SK., Whitesides GM., "Microfluidic devices fabricated in poly(dimethylsiloxane) for biological studies.", *Electrophoresis* 24.21 (2003): 3563-3576.
- [3] Psaltis D., Quake S., Yang C., "Developing optofluidic technology through the fusion of microfluidics and optics". *Nature* 442, 381-386 (27 July 2006).
- [4] Challa, P. K. Personal communication (2016).
- [5] Wolfe D. B., Conroy R. S., Garstecki P., Mayers B. T., Fischbach M. A., Paul K. E., Prentiss M., and Whitesides G. M., "Dynamic control of liquid-core/liquid-cladding optical waveguides," *Proc. Natl. Acad. Sci. U.S.A.* 101(34), 12434–12438 (2004).
- [6] Kirby, Brian J. *Micro-and nanoscale fluid mechanics: transport in microfluidic devices*. Cambridge University Press, 2010. p88.
- [7] Hessel, Volker, Schouten J. C., and Renken A., *Micro process engineering: a comprehensive handbook. Vol. 1*. John Wiley & Sons, 2009. p10.
- [8] Bergman, Theodore L., Frank P. Incropera, and Adrienne S. Lavine. *Fundamentals of heat and mass transfer*. John Wiley & Sons, 2011. pp406-409.
- [9] Tabeling, Patrick. *Introduction to microfluidics*. Oxford University Press, 2010. p118.
- [10] Feynman, Richard Phillips, Robert B. Leighton, and Matthew Sands. *Feynman Lectures on Physics. Vol. 1: Mainly mechanics, radiation and heat*. Addison-Wesley, 2011. §31-2
- [11] <http://cam.facilities.northwestern.edu/588-2/fluorescence-microscopy/> (Accessed 5/5/2016).
- [12] MicroChem Corporation, SU-8 3000 datasheet.
<http://microchem.com/pdf/SU-8%203000%20Data%20Sheet.pdf> (Accessed 5/5/2016).
- [13] <https://en.wikipedia.org/wiki/Photoresist> (Accessed 5/5/2016)

- [14] Nomada, Hiroaki, et al. "Carbon–polydimethylsiloxane-based integratable optical technology for spectroscopic analysis." *Talanta* (2015).
- [15] Tan, Say Hwa, et al. "Oxygen plasma treatment for reducing hydrophobicity of a sealed polydimethylsiloxane microchannel." *Biomicrofluidics* 4.3 (2010): 032204.
- [16] Eddington, David T., John P. Puccinelli, and David J. Beebe. "Thermal aging and reduced hydrophobic recovery of polydimethylsiloxane." *Sensors and Actuators B: Chemical* 114.1 (2006): 170-172.
- [17] Mata, Alvaro, Aaron J. Fleischman, and Shuvo Roy. "Characterization of polydimethylsiloxane (PDMS) properties for biomedical micro/nanosystems." *Biomedical microdevices* 7.4 (2005): 281-293.
- [18] Hale, George M., and Marvin R. Querry. "Optical constants of water in the 200-nm to 200-μm wavelength region." *Applied optics* 12.3 (1973): 555-563.
- [19] 3M Company, FC-40 datasheet.
<http://multimedia.3m.com/mws/media/648880/fluorinert-electronic-liquid-fc-40.pdf>
(Accessed 5/5/2016)
- [20] <http://www.sigmaaldrich.com/chemistry/solvents/methanol-center.html>
(Accessed 5/5/2016)
- [21] Moutzouris, Konstantinos, et al. "Refractive, dispersive and thermo-optic properties of twelve organic solvents in the visible and near-infrared." *Applied Physics B* 116.3 (2014): 617-622.
- [22] Pallas, N. R., and Y. Harrison. "An automated drop shape apparatus and the surface tension of pure water." *Colloids and surfaces* 43.2 (1990): 169-194.
- [23] Mazutis, Linas, and Andrew D. Griffiths. "Selective droplet coalescence using microfluidic systems." *Lab on a Chip* 12.10 (2012): 1800-1806.
- [24] Vazquez, Gonzalo, Estrella Alvarez, and Jose M. Navaza. "Surface tension of alcohol water+ water from 20 to 50. degree. C." *Journal of chemical and engineering data* 40.3 (1995): 611-614.
- [25] Feynman, Richard Phillips, Robert B. Leighton, and Matthew Sands. *The Feynman Lectures on Physics, Vol. 2: Mainly electromagnetism and matter*. Addison-Wesley, 2011. §32-5
- [26] <https://www.rp-photonics.com/fibers.html> (Accessed 5/5/16)
- [27] <https://en.wikipedia.org/wiki/Fluorescein> (Accessed 5/5/2016)
- [28] https://en.wikipedia.org/wiki/Fluorescence_microscope (Accessed 5/5/2016)
- [29] Charmet, Jérôme, Rupert Barton, and Michelle Oyen. "Tunable bioinspired lens." *Bioinspiration & biomimetics* 10.4 (2015): 046004.

[30] 3M Company, FC-72 datasheet.

<http://multimedia.3m.com/mws/media/648920/fluorinert-electronic-liquid-fc-72.pdf>

(Accessed 5/5/2016)